



Article

Isosteric Enthalpy Behavior of CO₂ Adsorption on Micro-Mesoporous Materials: Carbon Microfibers (CMFs), SBA-15, and Amine-Functionalized SBA-15

Reyna Ojeda-López ^{1,2} , Armando Domínguez-Ortiz ², Carlos Felipe ³ , A. Cervantes-Uribe ⁴, Isaac J. Pérez-Hermosillo ² and J. Marcos Esparza-Schulz ^{2,*}

- ¹ Laboratório de Pesquisa em Adsorção e Captura de CO₂ (LPACO2), Departamento de Engenharia Química, Universidade Federal do Ceará (UFC), Fortaleza 60455-760, Brazil; rol@xanum.uam.mx
 - ² Laboratorio de Físicoquímica de Superficies, Departamento de Química, Universidad Autónoma Metropolitana-Iztapalapa (UAM-I), Mexico City, CDMX 09340, Mexico; doar@xanum.uam.mx (A.D.-O.); ijph1986@gmail.com (I.J.P.-H.)
 - ³ Centro Interdisciplinario de Investigaciones y Estudios Sobre Medio Ambiente y Desarrollo (CIIEMAD), Departamento de Biociencias e Ingeniería, Instituto Politécnico Nacional (IPN), Mexico City, CDMX 07340, Mexico; cfelipe@ipn.mx
 - ⁴ Centro de Investigación de Ciencia y Tecnología Aplicada de Tabasco (CICTAT), Laboratorio de Nanomateriales Catalíticos Aplicados al Desarrollo de Fuentes de Energía, Universidad Juárez Autónoma de Tabasco (UJAT), Tabasco 86690, Mexico; adrian.cervantes@ujat.mx
- * Correspondence: esma@xanum.uam.mx



Citation: Ojeda-López, R.; Domínguez-Ortiz, A.; Felipe, C.; Cervantes-Uribe, A.; Pérez-Hermosillo, I.J.; Esparza-Schulz, J.M. Isosteric Enthalpy Behavior of CO₂ Adsorption on Micro-Mesoporous Materials: Carbon Microfibers (CMFs), SBA-15, and Amine-Functionalized SBA-15. *J. Compos. Sci.* **2021**, *5*, 102. <https://doi.org/10.3390/jcs5040102>

Academic Editor:
Francesco Tornabene

Received: 11 March 2021
Accepted: 4 April 2021
Published: 8 April 2021

Publisher's Note: MDPI stays neutral with regard to jurisdictional claims in published maps and institutional affiliations.



Copyright: © 2021 by the authors. Licensee MDPI, Basel, Switzerland. This article is an open access article distributed under the terms and conditions of the Creative Commons Attribution (CC BY) license (<https://creativecommons.org/licenses/by/4.0/>).

Abstract: The isosteric enthalpy of adsorption ($\Delta_{ads}\dot{h}$) of CO₂ in three different micro and mesoporous materials was evaluated in this work. These materials were a microporous material with functional groups of nitrogen and oxygen (CMFs, carbon microfibers), a mesoporous material with silanol groups (SBA-15, Santa Barbara Amorphous), and a mesoporous material with amine groups (SBA-15_APTES, SBA-15 amine-functionalized with (3-Aminopropyl)-triethoxysilane). The temperature interval explored was between 263 K and 303 K, with a separation of 5 K between each one, so a total of nine CO₂ isotherms were obtained. Using the nine isotherms and the Clausius–Clapeyron equation, the reference value for $\Delta_{ads}\dot{h}$ was found. The reference value was compared with those $\Delta_{ads}\dot{h}$ obtained, considering some arrangement of three or five CO₂ isotherms. Finally, it was found that at 298 K and 1 bar, the total amount of CO₂ adsorbed is 2.32, 0.53, and 1.37 mmol g⁻¹ for CMF, SBA-15, and SBA-15_APTES, respectively. However, at a coverage of 0.38 mmol g⁻¹, $\Delta_{ads}\dot{h}$ is worth 38, 30, and 29 KJ mol⁻¹ for SBA-15_APTES, CMFs, and SBA-15, respectively. So, physisorption predominates in the case of CMF and SBA-15 materials, and the $\Delta_{ads}\dot{h}$ values significantly coincide regardless of whether the isotherms arrangement used was three or five. Meanwhile, in SBA-15_APTES, chemisorption predominates as a consequence of the arrangements used to obtain $\Delta_{ads}\dot{h}$. This happens in such a way that the use of low temperatures (263–283 K) tends to produce higher $\Delta_{ads}\dot{h}$ values, while the use of high temperatures (283–303 K) decreases the $\Delta_{ads}\dot{h}$ values.

Keywords: isosteric enthalpy of adsorption ($\Delta_{ads}\dot{h}$); carbon microfibers (CMFs); SBA-15; SBA-15 functionalized with APTES; CO₂ adsorption; micro-mesoporous materials

1. Introduction

In recent years, various materials, both micro and mesoporous, have been studied for CO₂ capture, given the importance of removal and recovery from gas emissions. Many solid sorbents have been studied, such as activated carbon [1], polymers [2], molecular sieves [3], zeolites [4], Metal-Organic Frameworks (MOFs) [5], carbon nanofibers [6], carbon nanotubes [7], graphene [8], mesoporous silica [9], and functionalized silica oxides [10]. It is necessary for these solids to have a high adsorption capacity, accompanied with a low energy interaction in order to perform an efficient adsorbent. For this reason, understanding

the adsorption process is essential to determine the interaction between the adsorbent and the adsorbate. Furthermore, the adsorption process can be either physical (physisorption) or chemical (chemisorption): (i) Physisorption occurs whenever an adsorbable gas (the adsorptive) is brought into contact with the surface of a solid (the adsorbent), and (ii) chemisorption occurs where the intermolecular forces involved lead to the formation of chemical bonds [11]. Physisorption is accompanied by the low heat of adsorptions, with no violent or disruptive structural changes occurring to the surface during the adsorption measurement, which may lead to surface coverage by more than one layer of adsorbate [12], in the which the van der Waals interactions are involved [13]. Chemisorption, also called irreversible adsorption, is mainly characterized by large interaction potentials, which lead to the high heat of adsorption, often approaching the value of chemical bonds. As chemisorption occurs through chemical bonding, it is often found to occur at temperatures above the critical temperature of the adsorbate. Furthermore, chemisorption is necessarily restricted to, at most, a single layer of chemically bound adsorbate on the surface [12]. Then, a parameter that allows to distinguish between physisorption or chemisorption is the heat of adsorption.

The heat of adsorption is the thermodynamic property that describes the interactions between an adsorbent and an adsorbate [13–17]. The value of the heat of adsorption can be deduced from the adsorption isotherms obtained from at least two different temperatures. The energetic physisorption can be assessed directly by adsorption calorimetry: The curve obtained of *differential energies of adsorption* $\Delta_{ads}\dot{u}$ or *differential enthalpies of adsorption* $\Delta_{ads}\dot{h}$ (i.e., $\Delta_{ads}\dot{u} - RT$ for an ideal gas) vs. the amount adsorbed (n^a) allows one to study the energetics of surface coverage or micropore filling. However, the use of the term “*heat of adsorption*” is discouraged since it does not correspond to any well-defined thermodynamic change of state. The energetic data can also be assessed indirectly from adsorption isotherms obtained at different temperatures (i.e., the “*isosteric*” method, based on the use of the Clausius–Clapeyron equation) and this leads, for a given amount adsorbed, to the so-called “*isosteric heat*” (q_{st}). Strictly, this quantity is more meaningful than a simple “*heat*” since it is equal, with opposite sign, to $\Delta_{ads}\dot{h}$. For this reason, the term “*isosteric heat*” is preferably replaced by the term *isosteric enthalpy of adsorption*. For both experimental and theoretical reasons, the calorimetric method is considered more reliable than the isosteric method, mainly if one studies micropore filling or the adsorbate’s phase behavior” [11].

This work explores the measurement of isosteric enthalpy of adsorption as a measure of the surface affinity toward a specific gas (CO₂), reflecting the strength of interaction with the solid (carbon microfibers (CMFs), SBA-15, and SBA-15_APTES); it was calculated using the Clausius–Clapeyron equation [13–17]:

$$\Delta_{ads}\dot{h} = R \left[\frac{\partial \ln p}{\partial (1/T)} \right]_{\theta} \quad (1)$$

where $\Delta_{ads}\dot{h}$ is the isosteric enthalpy of adsorption, R is the ideal gas constant (8.314 J mol^{−1} K^{−1}), and θ is the gas (CO₂) surface coverage at a pressure p and temperature T .

By solving Equation (1), Equation (2) is obtained, where a plot of $\ln p$ versus $1/T$ gives a straight line with a slope of $\Delta_{ads}\dot{h} * R^{-1}$.

$$\ln p = - \frac{(\Delta_{ads}\dot{h})}{R} * \left(\frac{1}{T} \right) \quad (2)$$

Using Equation (2) and the CO₂ adsorption isotherms, different temperature combinations have been selected to evaluate the behavior of the isosteric enthalpy of adsorption on micro and mesoporous materials. The reference $\Delta_{ads}\dot{h}$ value is calculated using a total of nine isotherms at 263, 268, 273, 278, 283, 288, 293, 298, and 303 K. Then, different combinations are chosen within this temperature group, selecting only three or five isotherms. Depending on the interaction energy, the predominant process will be determined, either

physisorption or chemisorption. The materials evaluated in this work have different porosity, morphology, and chemical composition. The results obtained will be compared with results reported in other works on materials similar to those studied here.

2. Materials and Methods

2.1. Materials

Tetraethyl orthosilicate (TEOS, 98%), surfactant poly (ethylene glycol)-block-poly (propylene glycol)-block-poly (ethylene glycol) (P123), (3-aminopropyl) triethoxysilane (APTES, 99%), hydrochloric acid (36.5–38%), absolute ethanol (EtOH, 99.9%), polyacrylonitrile (PAN), and anhydrous N,N-dimethylformamide (DMF, 99.8%) were supplied by Sigma-Aldrich (Aldrich, St. Louis, MO, USA), and these were used as received without additional purification.

2.2. SBA-15 and SBA-15_APTES Synthesis

First, SBA-15 was prepared using the method reported by Zhao et al. [18]. Four grams of triblock copolymer Pluronic P-123 was dissolved in a solution of 120 g of deionized water and 24 g of 36.5–38.0% HCl under stirring until complete dissolution. Afterwards, 8.5 g of TEOS was added dropwise. The mixture was stirred at 313 K for 20 h and then was aged at 363 K for two days without mixing. The sample was recovered by filtration, washed with 150 mL of ethanol, and air-dried at 373 K for 24 h. The organic template was removed by calcination in air at 623 K in a tube furnace for 4 h [19].

Second, the functionalization of SBA-15 materials with APTES was performed with a ratio of 1:0.75, that is, 1 g of SBA-15 calcined at 623 K and 0.75 g of APTES. The SBA-15 sample was outgassed under vacuum at 373 K for 12 h to remove residual water, and then 100 mL of ethanol and the APTES were added with vigorous stirring. This process happens at 298 K and under a nitrogen atmosphere for 20 h [20].

2.3. Carbon Microfiber Synthesis

First, polyacrylonitrile microfibers (PANMFs) were synthesized using polyacrylonitrile (PAN) and N,N-Dimethylmethanamide (DMF) in a ratio of 0.1:0.9, a polymer concentration of 10%. The electrospinning apparatus was set at (i) flow rate of 1.0 mL/h, (ii) voltage of 15 kV and (iii) distance between the tip of the syringe and the collector of 10 cm. Then, the carbon microfibers were obtained by a calcination process that involved two phases: (i) Stabilization at 553 K (air atmosphere) for 30 min and (ii) carbonized at 1223 K (nitrogen atmosphere) for 90 min [21].

2.4. Characterization Techniques

2.4.1. Scanning Electron Microscopy (SEM) and Transmission Electron Microscopy (TEM)

SEM analysis was performed on a LEO 1450 VP electron microscope (Corbeil-Essonnes, Paris, France), operated at an acceleration voltage of 15 kV. Furthermore, TEM analysis was done on a High-resolution Transmission Electron Microscopy, HRTEM Jeol 2100F (Peabody, MA, USA), using a light source a field emitter and 200 kV acceleration. To measure microfiber diameters (CMF) and pore diameters (SBA-15 and SBA-15_APTES), the Comptage de particules-volume 2 software was used.

2.4.2. X-ray Diffraction (XRD)

Powder XRD patterns were recorded on a Bruker D8 Advance (Bruker, Billerica, MA, USA), using monochromatic $\text{CuK}\alpha$ radiation with a wavelength of 0.154 nm in (i) 0.6° to 5.0° in the 2θ scale (the low angle region) for SBA-15 and (ii) 5.0° to 70.0° for CMF.

In SBA-15 and SBA-15_APTES, it is possible to measure the pores thickness using Bragg's Law and consider the pore diameter obtained by nitrogen adsorption isotherms. Bragg's Law is giving by the following expression [22]:

$$n\lambda = 2 d_{hkl} \sin \theta \quad (3)$$

where λ is the X-ray wavelength, d_{hkl} is the spacing of the crystal layers (path difference), θ is the incident angle (the angle between the incident ray and the scattering plane), and n is an integer, in this case, $n = 1$.

From Equation (3) and using the incident angle, d_{hkl} it is obtained, and this value is used for calculating another parameter, a_0 , the distance between contiguous pore centers, which is important for determining the pore thickness. The equation is:

$$a_0 = \frac{(2)(d_{hkl})}{\sqrt{3}} \quad (4)$$

Finally, knowing the value of a_0 and the average pore diameter (obtaining by nitrogen adsorption), with Equation (5) it is finding the average pore wall thickness.

$$t_{pore} = a_0 - D_{pore} \quad (5)$$

2.4.3. Nitrogen Adsorption/Desorption (77 K)

The measurements were performed with a Micromeritics ASAP 2020 system (Micromeritics, Norcross, GA 30093, USA) at liquid nitrogen temperature (77 K). Before measurement, the samples were degassed at (i) 373.15 K for 12 h (SBA-15 and SBA-15_APTES) and (ii) 473.15 K for 12 h (CMF). The specific surface area was calculated by the multiple-point Brunauer–Emmett–Teller (BET) method. For mesoporous materials, the relative pressure interval using was 0.05 to 0.25 [11,23], and for microporous materials, the interval used was 0.005 to 0.1 [24]. Pore size distribution curves were computed by using the non-local density functional theory (NLDFT) method. Outgassing temperature was selected based on thermogravimetric analysis, and the SBA-15 and SBA-15_APTES materials were limited to a temperature of 373.15 K, sufficient to remove the physisorbed water but not to remove the organic matter from the amino groups in the SBA-15_APTES material (Figure S1); while for CMF, 473.15 K was selected, due to the high microporous nature and also the thermogram shows that it is thermally stable up to temperatures of 673.15 K (Figure S1).

2.4.4. Nuclear Magnetic Resonance (NMR)

Nuclear magnetic resonance (NMR) was performed in a Bruker Advance II300 spectrometer (NMR, Praha 6-Dejvice, Prague, Chequia Republic) operating at 59.62 MHz for ^{29}Si . The ^{29}Si was recorded by magic angle spinning (MAS) at 5 kHz. The ^{29}Si NMR spectra were referenced to tetramethylsilane.

2.4.5. X-ray Photoelectron Spectrometry (XPS)

X-ray photoelectron spectroscopy (XPS) was performed with a Thermo Scientific K-alpha spectrometer (XPS, Waltham, MA, USA) using monochromatic radiation $\text{AlK}\alpha$ source (1487 eV). The instrument base pressure was 1×10^{-9} mbar. The quantitative analysis was carried out using average spectra collected from different sample regions. The data were analyzed using the Thermo Avantage v5.932.

2.4.6. CO₂ Adsorption Measurement (263–303 K)

CO₂ adsorption isotherms were measured using a Quantachrome, Autosorb 1 (Autosorb, Boynton Beach, FL, USA). The presence of water in these materials was eliminated by heating to 473.15 K, at a rate of 1 K/min under vacuum (5×10^{-3} mmHg) overnight using the degassing system of *Autosorb 1*. The adsorption temperature was maintained (± 0.1 K) by circulating water/etilenglicol from a constant temperature bath MX07R-20 Model (PolyScience, Niles, Illinois, USA). The adsorbate gas (CO₂) was injected into the set up at volumes required to achieve a targeted group of pressures ranging from 0.001 to 1 bar with an equilibration time of 10 min at each point.

3. Results and Discussion

SEM images for materials micro-mesoporous can be observed in Figure 1. First, Figure 1(A1) shows an agglomerate of fibers, which are more perceptible in Figure 1(A2), and Figure 1(A3) shows one microfiber, where the average diameter for carbon microfibers oscillates between 200 and 400 nm. While SBA-15 and SBA-15_APTES do not show a significant change, they confirm the typical image of SBA-15 materials, and the important here is that the absence of agglomerates can be perceived in Figure 1C, which could be an indication that the APTES molecule only remains on the surface of the material and not inside the pores, after amine-functionalization. In order to show more significant changes in these materials, the TEM images will be presented.

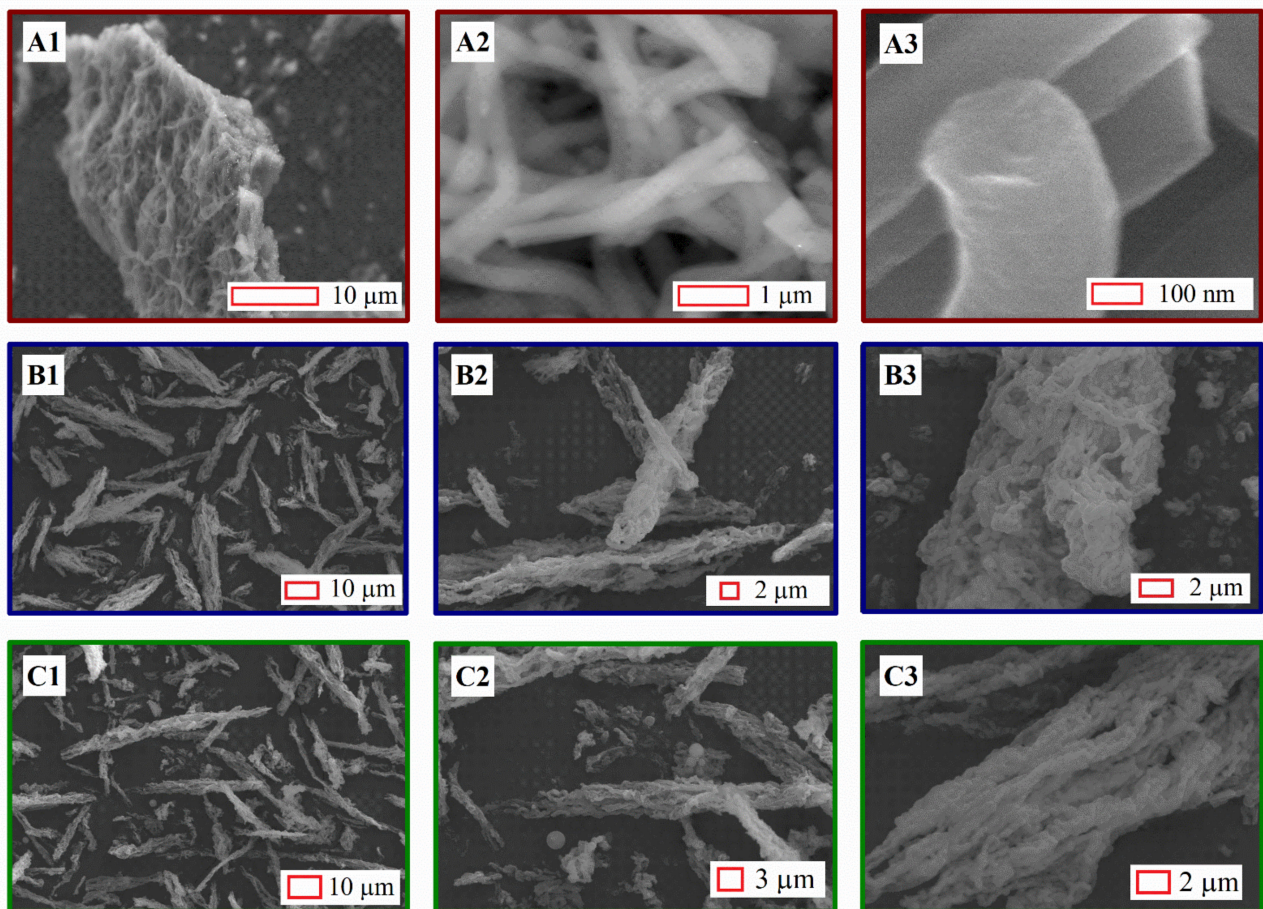


Figure 1. SEM images of (A) carbon microfibers, (B) SBA-15, and (C) SBA-15_APTES.

Figure 2 show TEM images of micro-mesoporous materials. The pores' morphology can be observed in them. In the case of CMFs, they have a pore arrangement of "shift pore" (Figure 2A); however, due to the temperature used for the calcination of CMFs, this material presents an amorphous arrangement, and it is necessary to use temperatures above 3000 K for these sheets to show a defined arrangement. Although it is difficult to make a precise measurement of the distance between each sheet, it can be confirmed that they are pores with less than 2.0 nm, which classifies it within the microporous materials, and the nitrogen adsorption can confirm this at 77 K and CO₂ adsorption at 273 K. SBA-15 and SBA-15_APTES have a hexagonal honeycomb arrangement (Figure 2B,C). The average pore diameters were obtained using the Comptage de particules-volume 2 software. The average diameter for SBA-15 fluctuates between 5.0 and 7.0 nm, while its thickness is between 3.0 and 5.0 nm. For SBA-15_APTES, the diameter varies from 4.0 to 5.0 nm and the thickness between 4.0 and 6.0 nm. Comparing these two materials, the pore diameter

decreases when the material is amine-functionalized with APTES, while the thickness increases. The above could indicate that a portion of the APTES molecule is efficiently fixed inside the pores of SBA-15.

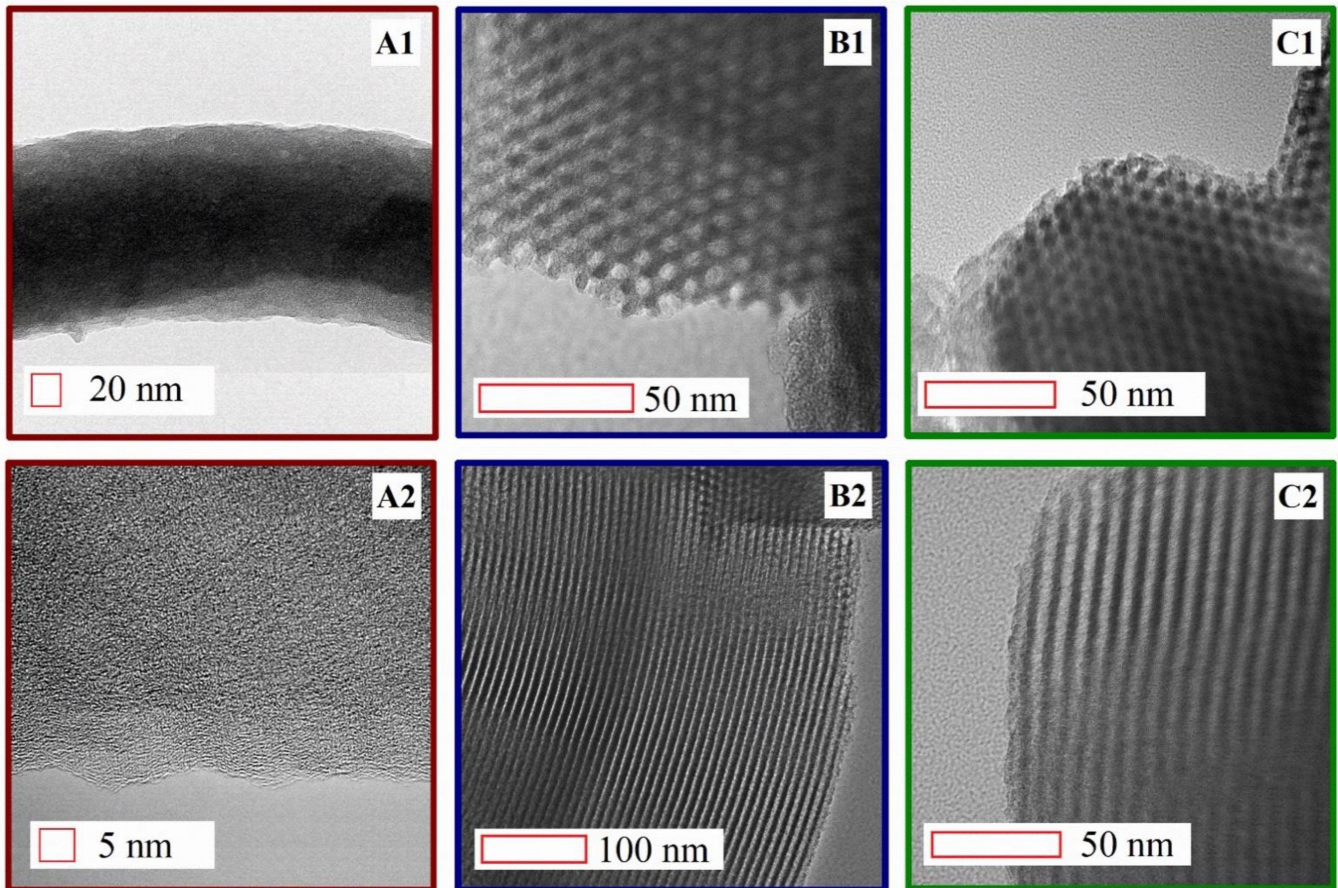


Figure 2. TEM images of (A) carbon microfibers, (B) SBA-15, and (C) SBA-15_APTES.

Figure 3 shows the diffractograms of the CMFs and SBA-15 materials. To CMFs, the signal at 25° in 2θ corresponds to the graphitic (002) planes [25–27], the high amplitude of the peak between 5° and 35° in 2θ indicates a high degree of amorphous on the graphene sheets. When the materials are calcinated at temperatures above 1223 K, the graphitization is promoted and it will be observed in the signal in (100), attributed to the lateral extent of graphitic domains. Remembering that SBA-15 materials have a defined arrangement, for XRD, it is necessary to work at a low angle, on a scale of 0.5° to 5° . Both materials have similar XRD diffraction patterns, they have three peaks associated with refraction planes (100), (110), and (200). These peaks indicate a hexagonal arrangement of cylindrical mesopores, the characteristic structure of SBA-15 materials; however, it is possible to note that SBA-15_APTES has shifted to the left. The geometric parameters of the mesopore hexagonal arrangement in the plane (100) are calculated following Kruk et al. [28,29], and they are presented in Table 1. From angle 2θ in Figure 3, d_{100} (the spacing of the crystal layers) and a_0 (distance between contiguous pore centers) were calculated. These two parameters, and using the average diameter calculated from the nitrogen isotherms, allow the pore thickness to be calculated, obtaining 3.5 nm and 5.8 nm for SBA-15 and SBA-15_APTES, respectively. These values present the same tendency as the values observed with TEM images; the pore wall thickness decreases when the SBA-15 is amine-functionalized.

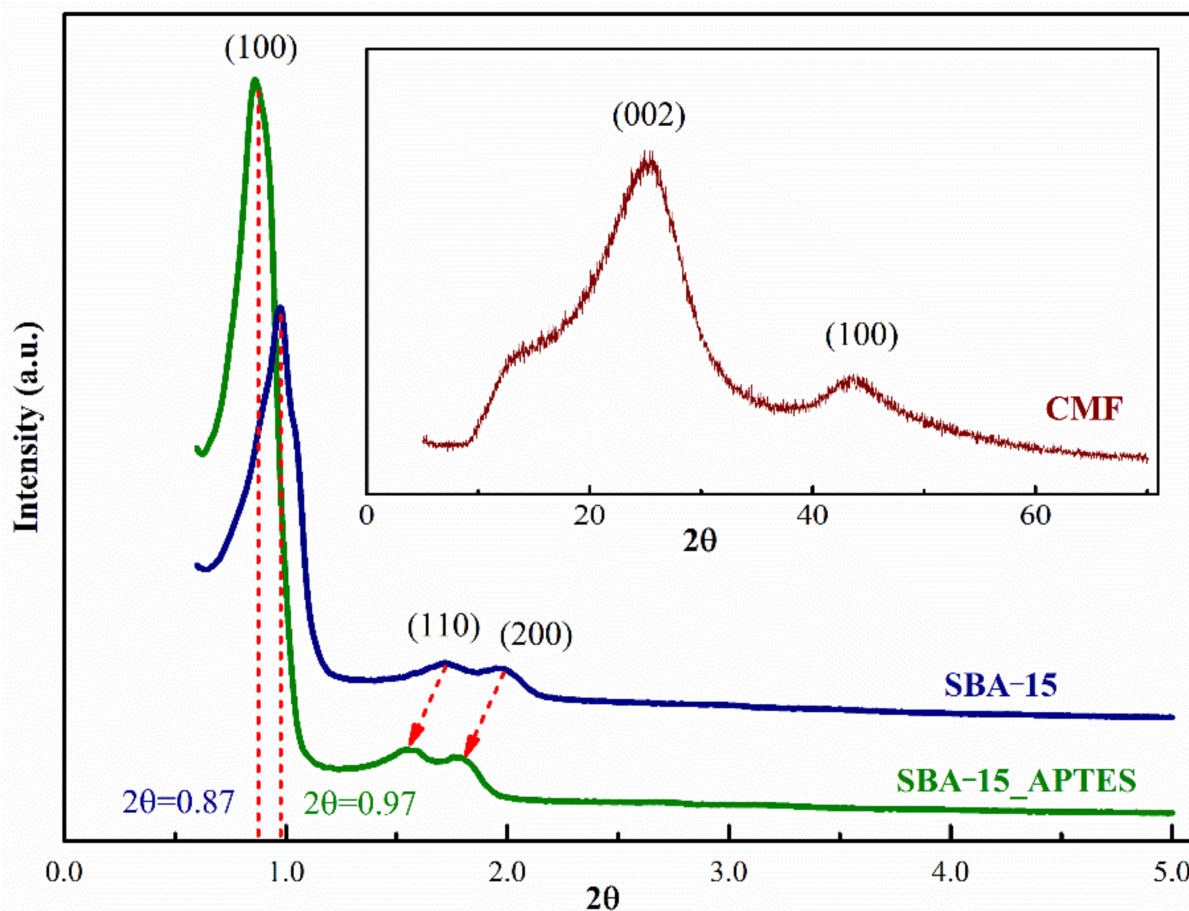


Figure 3. Powder XRD diffraction patterns of micro-mesoporous materials.

Table 1. Textural properties of SBA-15, SBA-15_APTES, and carbon microfibers (CMFs).

Name	CMF	SBA-15	SBA-15_APTES
d_{100} (nm)	—	9.097	10.142
a_0 (nm)	—	10.504	11.711
t_{pore} (nm)	—	3.474	5.830
S_{BET} (m ² /g)	805	735	389
S_{MICRO} (m ² /g)	753.2	193.2	0
S_{EXT} (m ² /g)	51.9	541.8	389
V_T (cm ³ /g)	0.3402	0.9336	0.5362
V_{MICRO} (cm ³ /g)	0.3007	0.09422	0
% M	88	10	0
D_{PORE_N2} (nm)	0.78	7.03	5.88
D_{PORE_CO2} (nm)	0.50	—	—

d_{100} ≡ the spacing of the crystal layers; a_0 ≡ distance between contiguous pore centers; t_{pore} ≡ pore wall thickness; S_{BET} ≡ surface specific area by BET equation; S_{MICRO} ≡ microporous area by t-plot method; S_{EXT} ≡ external surface area; V_T ≡ total volume at 0.95 in relative pressure; V_{MICRO} ≡ microporous volume by t-plot method; % M ≡ % of microporosity using total volume and microporous volume; D_{PORE_N2} ≡ average pore diameter calculated using nitrogen isotherms at 77 K; D_{PORE_CO2} ≡ average pore diameter calculated using CO₂ isotherms at 273 K.

The textural properties were calculated by nitrogen adsorption at 77 K. Figure 4 shows the isotherms obtained. CMFs present a combined isotherm between Type I(A) (microporous) and Type IV (mesopores), with a narrow hysteresis loop H1, which is typical of slit-like larger pores in activated carbons [11]. In general, the adsorbed volume at a relative pressure of less than 0.1 indicates that the material is mostly microporous, i.e., at least 80% corresponds to microporous. In contrast, SBA-15 and SBA-15_APTES show an isotherm type IV with a hysteresis loop, H1, characterized by mesoporous materials. In

both materials, the left shift of the hysteresis cycle of the SBA-15_APTES is very noticeable with respect to the SBA-15. This shift indicates a diminution in the average pore diameter, and it will be observed with the pore size distribution (PSD) in Figure 5. In addition, it is possible to note that the amount adsorbed decrease, which can be for two reasons: (i) An efficient amine-functionalization with APTES, or (ii) a pore blockage. The latter is more likely to occur in micropores due to the kinetics of the APTES molecule.

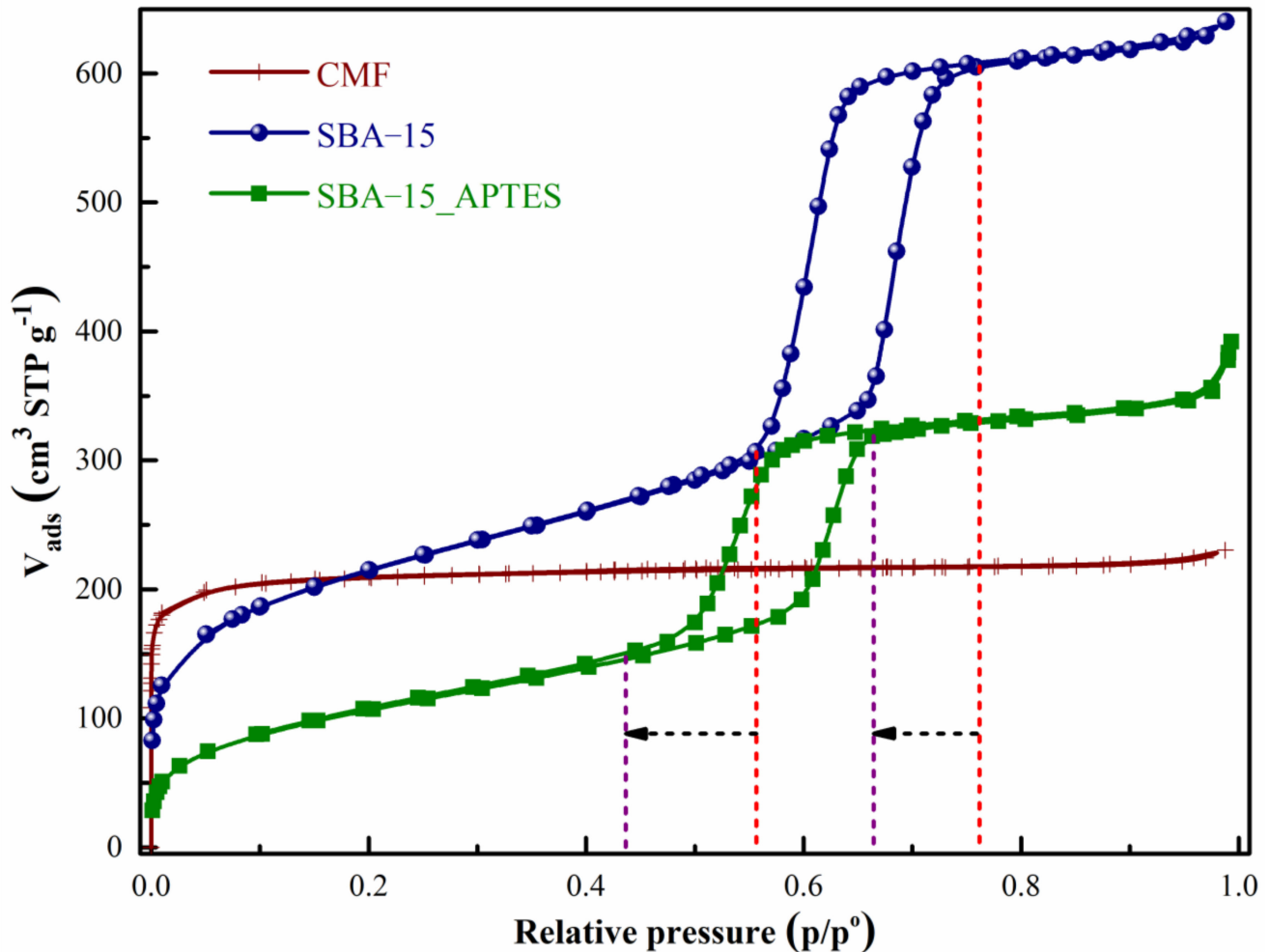


Figure 4. Nitrogen adsorption/desorption of micro-mesoporous materials.

The pore size distribution (PSD) shown in Figure 5 is calculated by non-local density functional theory (NLDFT) using the nitrogen isotherms of Figure 4. The PSD for CMFs confirms its microporosity, with an average pore diameter between 0.7 and 2.0 nm, predominantly pores of 0.8 nm. However, following the recent research recommendations for carbon materials, in CO₂ adsorption isotherms at 273 K, the diffusion is much faster and pores as small as 0.4 nm can be accessed [11]. So, in the upper part of Figure 5, it shows the PSD calculated by the CO₂ isotherm at 273 K. Here, it can be observed that the average pore diameter for CMFs oscillates between 0.4 and 0.8 nm, and the CO₂ isotherm allows the identification of pores smaller than the N₂ isotherm. The PSD for SBA-15 and SBA-15_APTES is shown the interval of mesoporous, with SBA-15 from 6.0 nm to 8.0 nm and SBA-15_APTES between 5.0 nm and 7.0 nm. Considering the pore width mode, 7.0 nm for SBA-15 and 5.9 nm for SBA-15_APTES, there is a diminution of ~1.1 nm; this could be due to the APTES molecules anchored on the surface of the SBA-15 pores, and if this is the case, CO₂ adsorption corroborates this observation. Although it is a very small amount, the

SBA1-15 sample shows the presence of micropores, which have been completely blocked when the sample is functionalized (SBA-15_APTES).

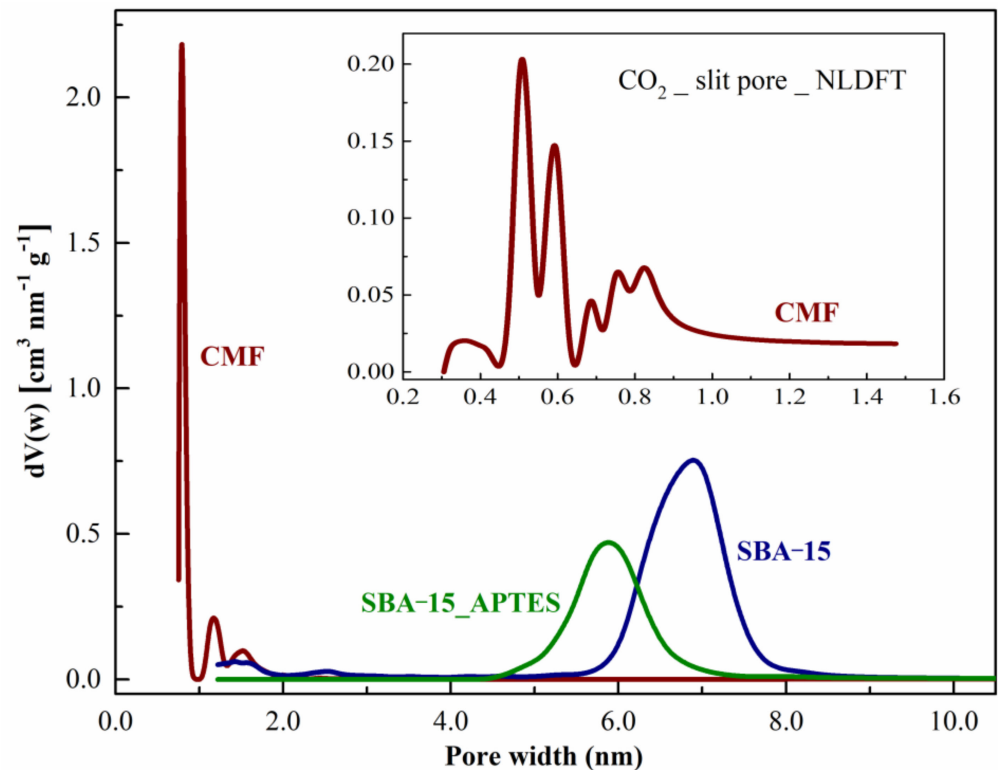


Figure 5. Non-local density functional theory (NLDFT) model pore size distribution of micro-mesoporous materials.

The textural properties calculated by XRD and N_2 adsorption are described in Table 1. By XRD, a diminution of thickness is observed for SBA-15 and SBA-15_APTES materials. The specific surface area for CMFs is a value close to SBA-15, $805 \text{ m}^2 \text{ g}^{-1}$ and $735 \text{ m}^2 \text{ g}^{-1}$, respectively, the first a microporous material and the second a mesoporous material. The surface area for SBA-15_APTES decreases up to $389 \text{ m}^2 \text{ g}^{-1}$, approximately 47% with respect to SBA-15. From the micropores volume and total volume, the percentage of microporosity is calculated, 88% for CMFs and 10% for SBA-15; in SBA-15_APTES, there are no presence of micropores, as they were probably blocked by the APTES molecule.

In general terms, the chemical composition of these three materials can be evaluated by XPS (CMF) or ^{29}Si RMN (SBA-15 and SBA-15_APTES). CMFs are composed of 91% carbon, 5% nitrogen, and 4% oxygen (Figure 6). Then, CMFs are a microporous material with functional groups of nitrogen and oxygen; these groups can allow a better interaction between CO_2 molecules and CMFs. Some of these species are pyrrolic-N/pyridine, quaternary-N or graphitic-N, pyridine-N-oxide, carbonyl (C=O), and C-O bonds; it is suggested that these groups help to increase the adsorption of CO_2 [27].

Silicon materials were evaluated by ^{29}Si RMN. SBA-15 is characterized by the presence of silanol groups (Si-OH bonds) and siloxanes (Si-O-Si bonds), which are labelled as “Q” in NMR. When SBA-15 is amine-functionalized, they also present “T” sites, the R-Si bonds (where R represents an organic residue) present in APTES molecules (top of Figure 6); the presence of these groups indicates a good impregnation of APTES on SBA-15. Q^2 (geminal silanols), Q^3 (free and vicinal silanols), and Q^4 (siloxane) sites are assigned at chemical displacements $\delta = -93$, -103 , and -112 ppm, respectively [19,20,30–32]. SBA-15_APTES present: (i) A decrease in Q^2 and Q^3 signals, which are associated with the loss of silanol groups, and (ii) an increment in Q^4 , related to the condensation of silanol groups to form siloxane groups. In addition to these changes, in the graph for SBA-15_APTES, two signals

can be perceived, corresponding to T^2 ($\text{SiR}(\text{OSi})_2(\text{OH})$ groups) and T^3 ($\text{SiR}(\text{OSi})_3$ groups) bands, assigned at $\delta = -60$ y -68 ppm, respectively [19,20,30–32]. It could be proposed that these signals are indicating a good impregnation of APTES molecules. However, it is also possible the interaction is between APTES molecules [20]. Then, the results regarding CO_2 adsorption could give a better idea, especially concerning the isosteric enthalpy of adsorption, which will determine the interaction energy between the solid and the CO_2 molecule, resulting in physisorption or chemisorption.

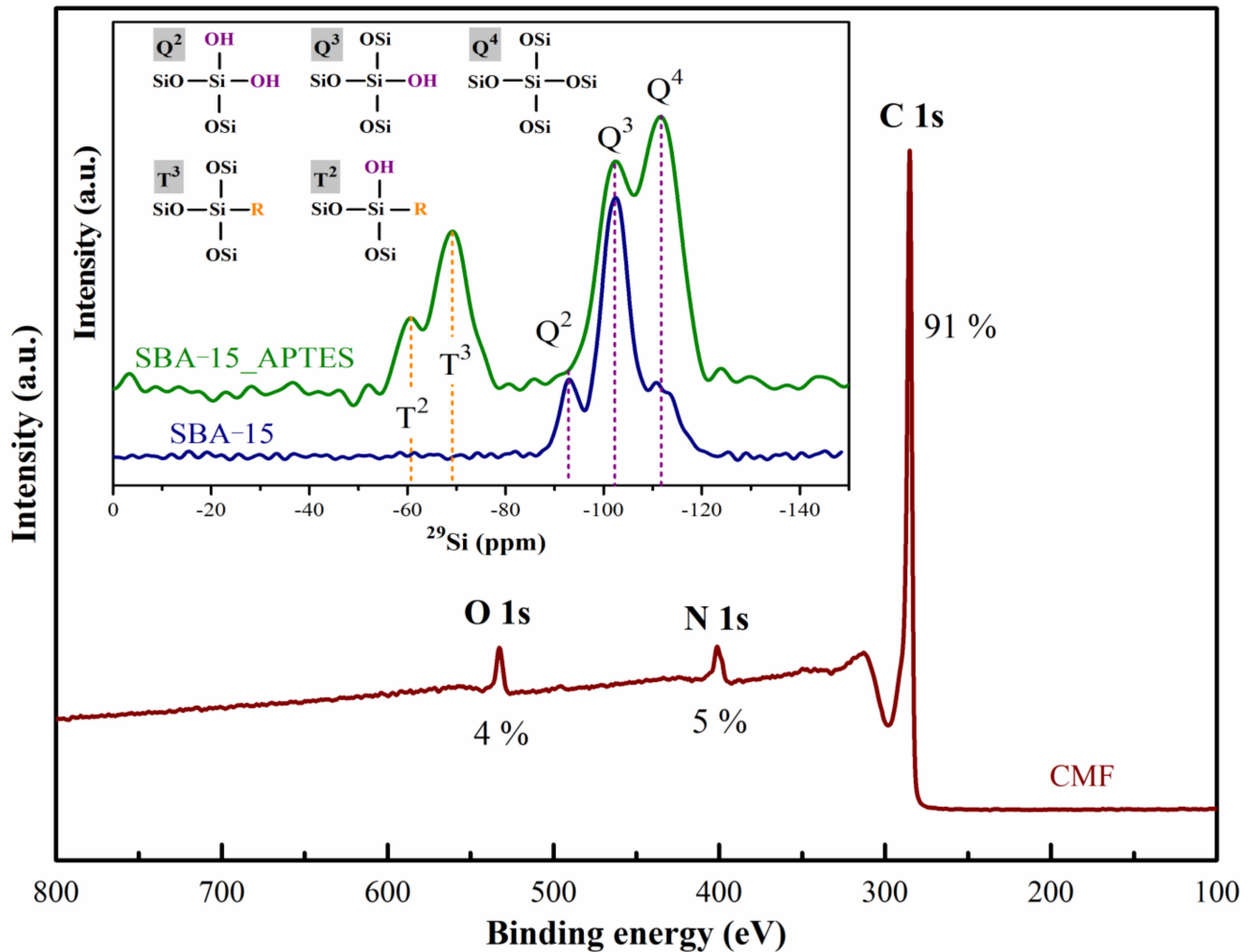


Figure 6. XPS for CMFs and ^{29}Si NMR for SBA-15 and SBA-15_APTES materials.

By means of different characterization techniques, the textural, structural, and chemical properties have been studied for the three materials: CMFs, SBA-15, and SBA-15_APTES. Now, we present the analysis of the variation in the value for $\Delta_{ads} \dot{h}$ using different combinations of the temperature for the CO_2 isotherms. The point of reference will be the curve obtained for $\Delta_{ads} \dot{h}$ when nine isotherms were considered. Table 2 shows the selected arrangements, considering intervals of 5 K, 10 K, or 20 K, selecting towards lower or higher temperatures, within the studied interval (263 K to 303 K). The effect of the microporosity and chemical composition will be reflected in the results shown below.

Table 2. Arrangements selected in the range from 263 K to 303 K.

	263 K	268 K	273 K	278 K	283 K	288 K	293 K	298 K	303 K
1	x	x	x	x	x	x	x	x	x
2	x		x		x		x		x
3	x	x	x	x	x				
4					x	x	x	x	x
5			x	x	x	x	x		
6	x				x				x
7	x		x		x				
8					x		x		x
9			x		x		x		
10	x			x			x		
11	x	x	x						
12			x		x			x	

The calculation procedure for the isosteric enthalpy of adsorption is described below. Nine isotherms were obtained at 263, 268, 273, 278, 283, 288, 293, 298, and 303 K. Figure 7 shows the nine isotherms of CO₂ at different temperatures for a microporous material (CMF). Here, diverse cuts are made at constant volume. When using Equation (2), there are two restrictions for these cuts: (i) At low pressures and (ii) at high pressures. The isotherm will define the smallest value that will be considered for the volume at the lowest temperature (263 K) because this is the temperature at which the largest amount of CO₂ is adsorbed (zoom Figure 7, the box on the bottom right). Besides, the largest value will be determined by the isotherm of the highest temperature (303 K), which adsorbed the minimum amount of CO₂ (Figure 7). Considering this interval, different cuts are realized; a segment provides a slope and a slope value of the $\Delta_{ads}h$ for each selected volume. The greater the number of slices made, the more defined the result, usually at low coverages.

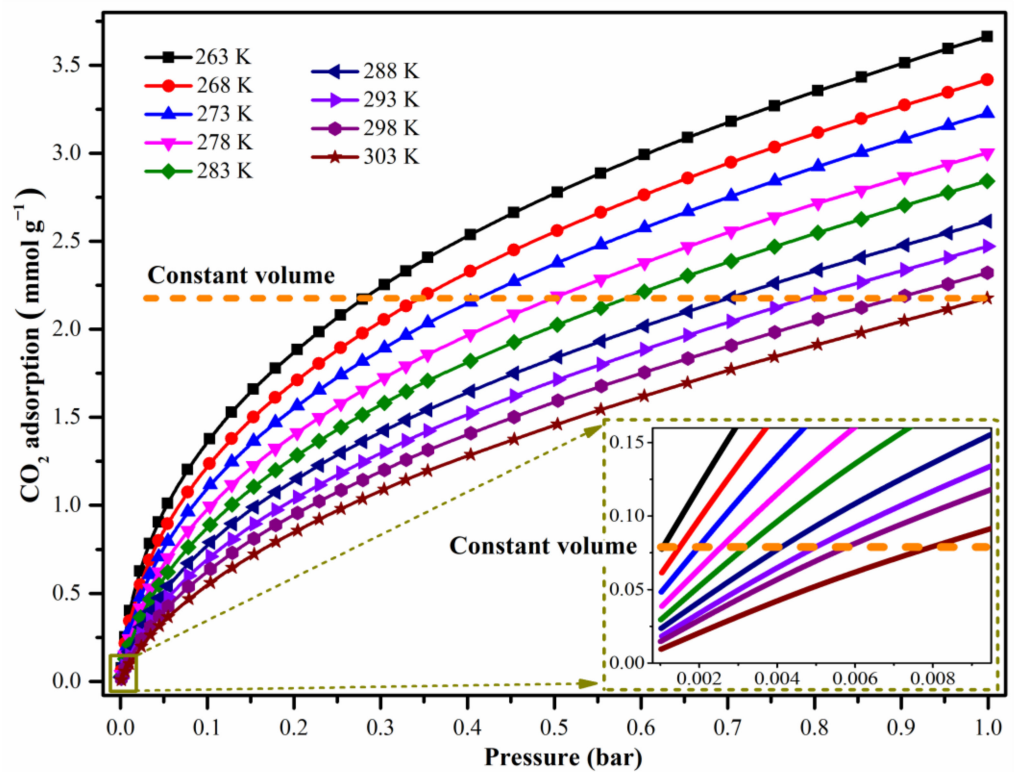


Figure 7. CO₂ isotherms of carbon microfibers calcined at 1223 K.

In addition to allowing the calculation of the isosteric enthalpy of adsorption, the isotherms in Figure 7 show the CO₂ adsorption capacity on CMFs. At 298 K and 1 bar, CMFs adsorbed 2.32 mmol g⁻¹, and this is comparable with other studies that synthesized carbon microfibers using PAN as a precursor and the electrospinning method. For example, Chiang et al. synthesized carbon nanofibers (CNF) with a specific surface area of 306 m² g⁻¹ and an adsorption of 2.52 mmol CO₂ g⁻¹ [33]. Heo et al. explored CNF with and without activation, CNF and ACNF, respectively; CNF presented a small area (12 m² g⁻¹) and small adsorption (0.55 mmol CO₂ g⁻¹), while ACNF with area of 925 m² g⁻¹ had an adsorption of 2.21 mmol CO₂ g⁻¹ [34]. Jeong et al., prepared CNFs added melamine, but the material without melamine named MACNF-0 with a specific surface area of 412 m² g⁻¹, at 273 K and 1 bar adsorbed 1.61 mmol CO₂ g⁻¹ compared with 3.22 mmol CO₂ g⁻¹ for CMF (synthesized in this work) at the same conditions [35]; an enhanced adsorption in this case may be due to the presence of nitrogen and oxygen functional groups.

Using the procedure explained above, Figure 8 shows the CO₂ isosteric enthalpy of adsorption ($-\Delta_{ads}h$) is in the interval of 35 and 20 kJ mol⁻¹ at various CO₂ adsorbed loadings. These values are slightly higher than those reported for carbon materials (~25 kJ mol⁻¹) that do not contain nitrogen and oxygen functional groups [36]: This implies a strong interaction between nitrogen and oxygen species with CO₂ molecules, demonstrating the surface heterogeneity and developed surface chemistry of the synthesized adsorbents, in addition to the presence of microporous [37,38]. It is essential to mention that these values are within the range for physical adsorption, which allows for easy regeneration of the materials [12,39]. Chiang et al. explored different carbonization temperatures for carbon nanofibers (CNF) and a tendency is observed in the isosteric enthalpy of adsorption, where the materials with a higher $\Delta_{ads}h$ value are those that were carbonized at lower temperatures. Moreover, based on their XPS results, these materials present a higher amount of nitrogen and oxygen, which means that the presence of these groups allows a higher surface affinity between the adsorbate and the adsorbent [33].

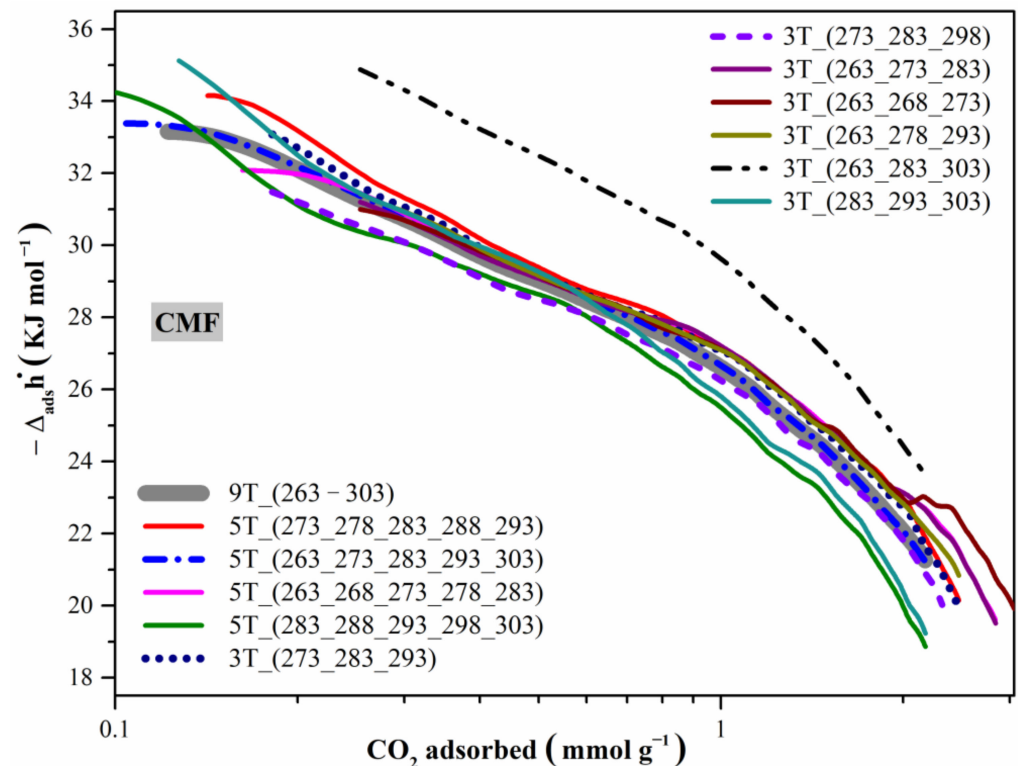


Figure 8. CO₂ isosteric enthalpy of polyacrylonitrile microfibers (PANMF) carbonized at 1223 K.

Independently of the selected arrangement, the trend in the ($\Delta_{ads} \dot{h}$) values does not present significant changes (Figure 8), except for arrangement 3T (263, 283, 303), where the temperature difference between each isotherm is 20 K. The above means that the more significant the temperature difference between the isotherms used, the greater the reference values' deviation. Two arrangements perform best and can be recommended when it is not possible to obtain nine isotherms: (i) Five isotherms (if it is possible to obtain five measurements, then it is recommended to use 263, 273, 283, 293, and 303 K) and (ii) three isotherms (if it is only possible obtain three isotherms, then it is recommended to use 273, 283, and 293 K).

Figure 9 shows the CO₂ isotherms of SBA-15. Note that the amount adsorbed at 263 K is ~ 1.1 mmol g⁻¹, a value three times smaller than the value for CMFs, 3.5 mmol g⁻¹ at 263 K. Ribeiro et al. reported 0.59 mmol g⁻¹ at 303 K and 1 bar against a value of 0.47 mmol g⁻¹ for the material synthesized here [40]. The isotherms in Figure 9 show a decrement in the amount of CO₂ adsorbed with an increase of temperature and at 298 K SBA-15 adsorb ~ 0.53 mmol g⁻¹, a quantity too small to be considered a material of interest for CO₂ capture. However, in addition to its thermal and mechanical stability and its high surface area, it has silanol groups that allow interaction with other molecules that are more akin to the CO₂ molecule. For this reason, the addition of an amine-functionalized material is vital in this study.

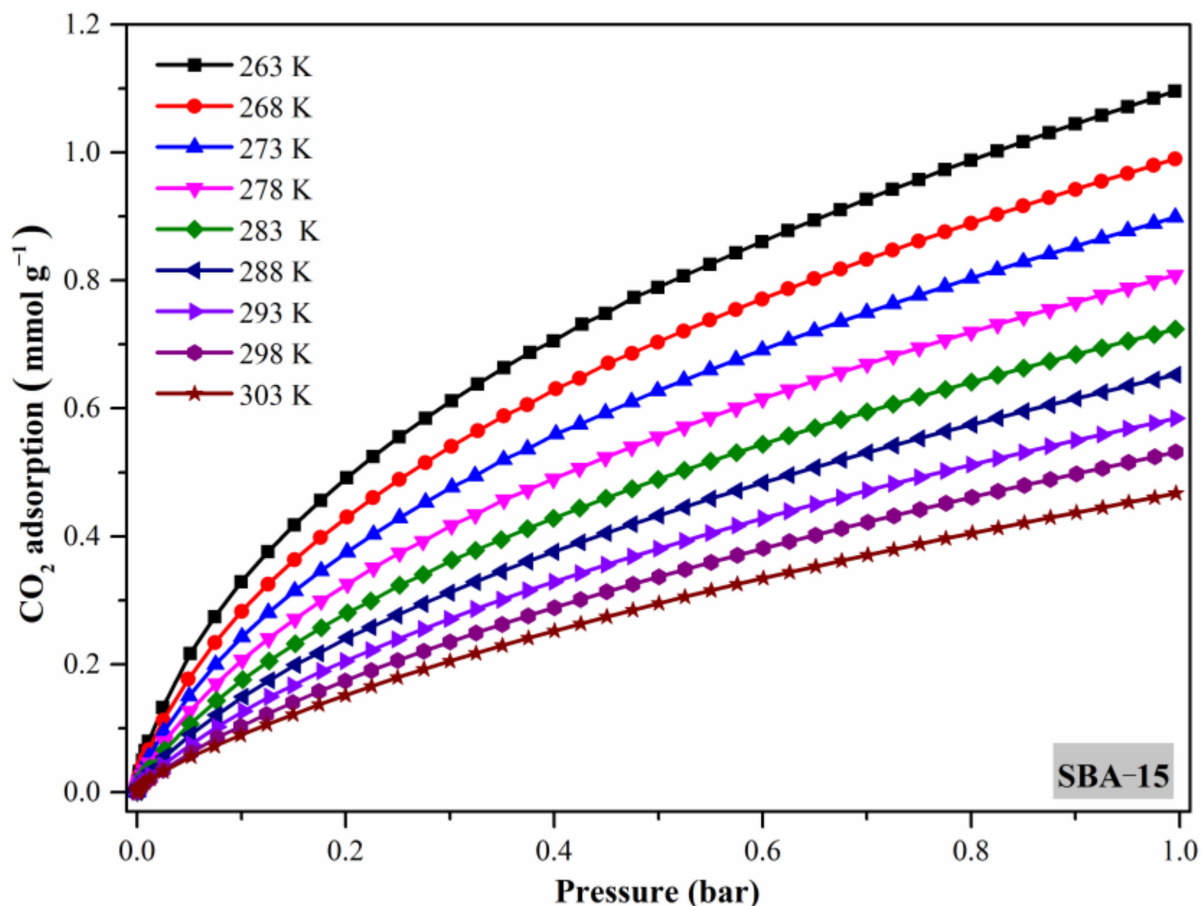


Figure 9. CO₂ isotherms of SBA-15 calcinated at 623 K.

The isosteric enthalpy of adsorption presents a similar value at low coverages (Figure 10) with respect to CMF. For SBA-15, the isosteric enthalpy of adsorption of CO₂ decreased with the coverage increased, meaning this is a material with heterogeneity in the adsorption sites. Furthermore, considering that as the pressure increases, a multilayer begins to form, in that case, adsorbate–adsorbate interactions are weaker, leading to a decrease in the

$\Delta_{ads}h$ value. The highest value occurs at low pressures, where the interaction is adsorbate–adsorbent, and it is here where the strongest interaction is found. As with CMFs, the $\Delta_{ads}h$ values are within the physisorption interval. Most of the selected arrangements show similar behavior with the reference value, except again for the arrangement with a difference of 20 K between each chosen temperature (263 K, 283 K, and 303 K). Three arrangements exhibit atypical behavior. This is the case when choosing either the upper end of temperatures or only the lower end. Here, it is crucial to select an interval that includes low and high temperatures. Even so, the deviation does not exceed 5%.

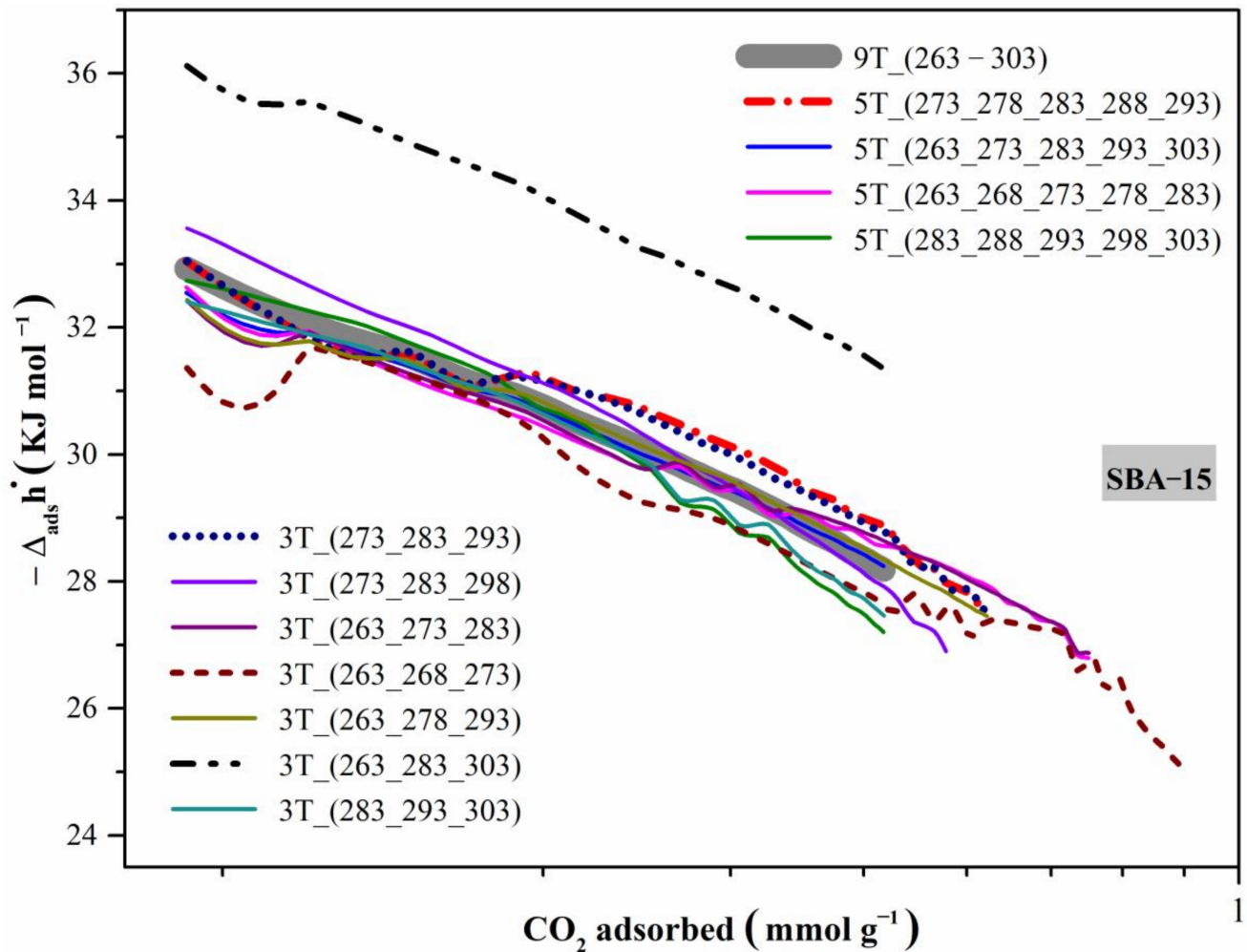


Figure 10. CO₂ isosteric enthalpy of SBA-15 calculated at 623 K.

Finally, the behavior of the modified material will be analyzed in Figure 11. The amount of CO₂ adsorbed has increased, and the difference between each of the isotherms is smaller than the isotherms of the SBA-15 material. At 298 K, the amount adsorbed is 1.37 mmol g⁻¹, increasing 150% more than its source material, SBA-15 (0.53 mmol g⁻¹). This increase may be because the silanol groups (surface chemical of SBA-15) interacted with the APTES molecule, forming amine groups that are more affine to CO₂; at low pressures, a higher adsorbed quantity can be perceived. Table 3 presents a comparative analysis between the results obtained in this work and other studies reporting SBA-15 functionalized with amine groups. Although the same agent is used for functionalization, there may be some variations, which depend on the amount of APTES used, but especially on the solvent used, which also has a strong influence during the impregnation process. However, in general, the values range very close to the results obtained here.

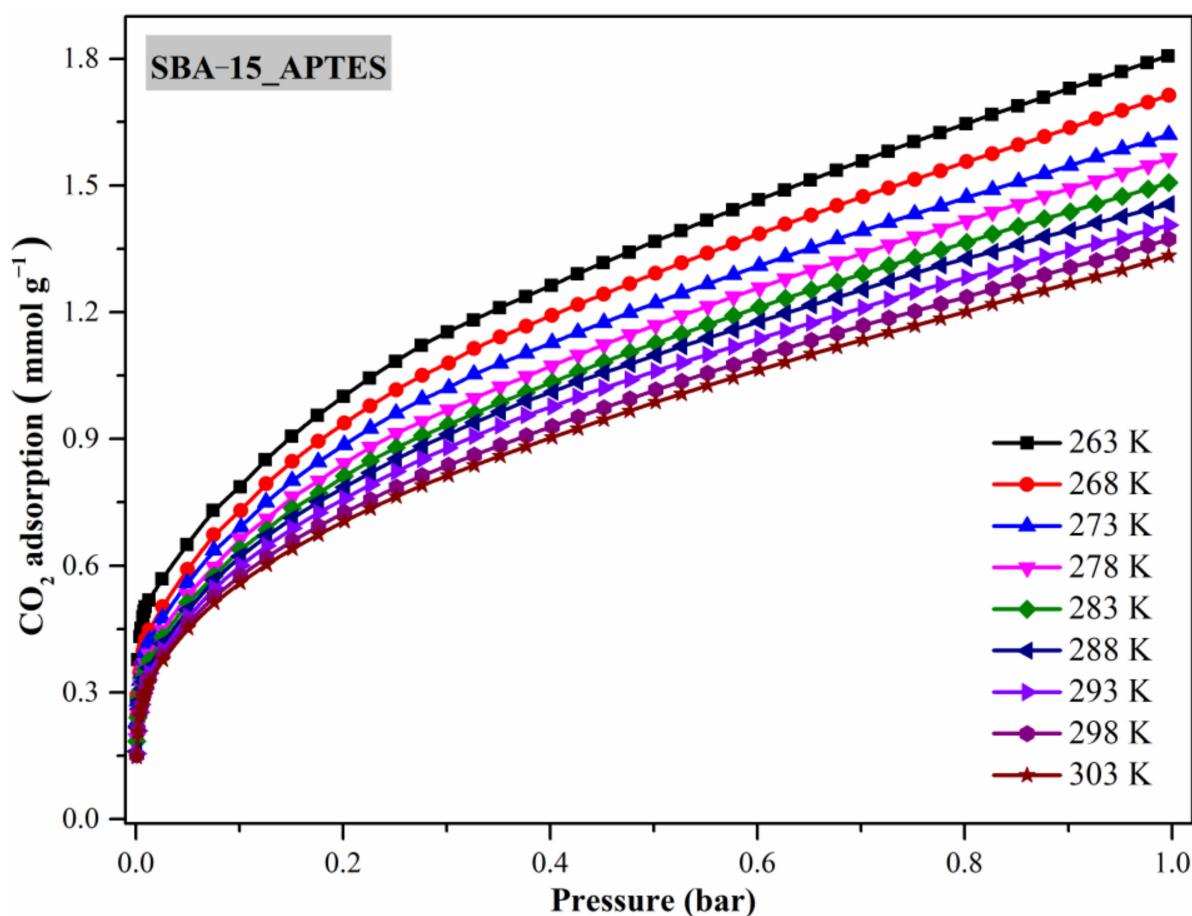


Figure 11. CO₂ isotherms of SBA-15 calcinated at 623 K and functionalized with (3-Aminopropyl)triethoxysilane (APTES).

Table 3. Comparison of the CO₂ adsorbed between samples reported in this work and other studies.

Adsorbent	Functionalizing Agent	Solvent	S _{BET} (m ² g ⁻¹)	Temperature (K)	CO ₂ Adsorbed (mmol g ⁻¹)	REF
SBA-15	—	—	735	298	0.53	This work
SBA-15	APTES ¹	Ethanol	389	298	1.37	This work
SBA-15	—	—	735	303	0.47	This work
SBA-15	APTES	Ethanol	389	303	1.34	This work
SBA-15	—	—	572	303	0.59	[40]
SBA-15	APTES	Ethanol	276	303	0.84	[40]
SBA-15	APTES	Toluene	50	303	1.43	[40]
SBA-15	APTES	Toluene	216	298	2.12	[41]
SBA-15	PEI ²	Methanol	267	298	1.74	[41]
SBA-15	APTES	Toluene	150	298	1.33	[42]
SBA-15	PEI	Methanol	49	298	1.33	[42]
SBA-15	—	—	696	293	1.1	[43]
SBA-15	APTES	Toluene	361	298	1.1	[43]
SBA-15	—	—	793	298	0.91	[20]
SBA-15	APTES	Toluene	223	298	1.43	[20]
SBA-15	APTES	Ethanol	356	298	1.40	[20]

¹ (3-Aminopropyl)-triethoxysilane (APTES); ² Polyethylenimine-ethylenediamine (PEI).

Figure 12 show the isosteric enthalpy of adsorption of CO₂ for SBA-15_APTES. We can observe two trends: (i) The $\Delta_{ads}h$ begins at values greater than 40 KJ mol⁻¹, which implied a chemisorption process, and (ii) the arrangements show very significant differences. First, what is the reason for high values? One assumption is that there are enough amine groups at low coverages to interact with CO₂ and adsorb it, but there are only enough for a first layer. When all these sites are occupied, the interaction is only adsorbate-adsorbate; consequently, isosteric enthalpy of adsorption decreases. Unlike CMFs and

SBA-15, where the 3T (263_283_303) arrangement deviated more from the reference value, here it is one of the arrangements that is recommended, along with the five-temperature arrangement that covers the full range of study in this work (5T_(263_273_283_293_303)). The three arrangements that show a big deviation of the reference value included the lowest temperatures, which is normal considering that obtaining $\Delta_{ads}\dot{h}$ depends on the isotherm that presents the least amount of adsorption at low pressures. When considering the 3T_(263_238_263) > 3T_(263_273_283) arrangements, the isotherms adsorb considerably more CO₂ compared to the arrangements that include higher temperature isotherms; this causes the $\Delta_{ads}\dot{h}$ values to be larger. On the contrary, when working with arrangements such as 3T_(283_293_303), with higher temperatures, the $\Delta_{ads}\dot{h}$ values decrease based on the reference value; in this case, at low pressures, these temperatures adsorb a lower amount of CO₂. Here it is very important to consider choosing temperatures that include a greater interval between low and high temperatures. $\Delta_{ads}\dot{h}$ deviates towards very high values if low temperatures are chosen, and if very high temperatures are chosen, $\Delta_{ads}\dot{h}$ deviates towards very small values.

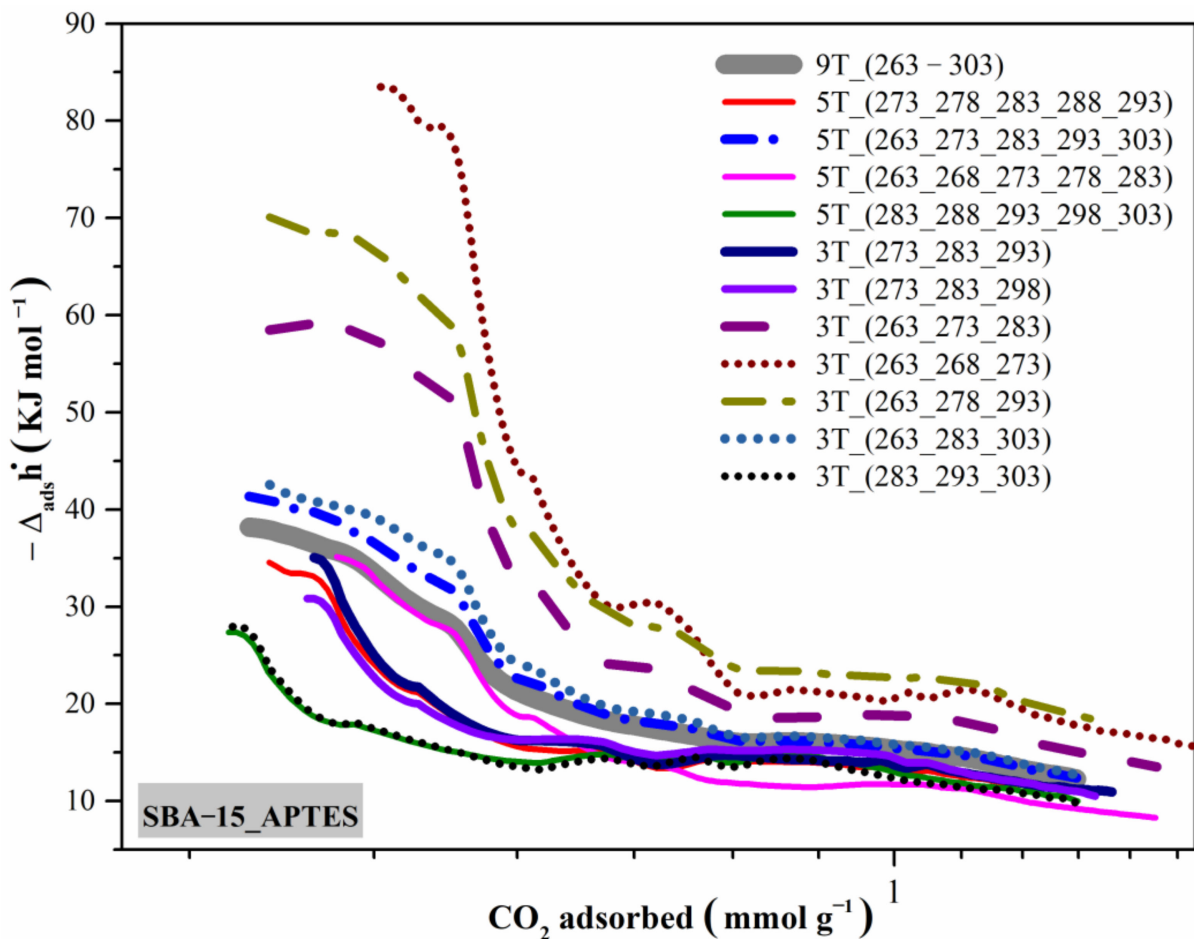


Figure 12. CO₂ isosteric enthalpy of SBA-15 calcinated at 623 K and functionalized with APTES.

The three materials were compared, considering the CO₂ isotherms and the $\Delta_{ads}\dot{h}$ in Figure 13. One can see that at 298 K, CMFs with a specific surface area of 805 m² g⁻¹ adsorb 2.3 mmol g⁻¹ and SBA-15 with 735 m² g⁻¹ of area adsorbs 0.53 mmol g⁻¹; both materials have a comparable specific surface area, and the specific surface area is not the determining factor for better CO₂ adsorption. There are two differences between these materials: CMFs are microporous with nitrogen and oxygen functional groups, while SBA-15 is mesoporous with OH functional groups. The chemical composition plays the

most essential role in this process, but does microporosity also play a role? Some carbon materials with similar textural characteristics but without nitrogen and oxygen functional groups or a smaller quantity of these materials adsorb lower amounts of CO₂ [44]; therefore, the influence of micropores could be excluded. Now, SBA-15_APTES has a specific surface area of 389 m² g⁻¹ (practically half of the other materials), and it adsorbs less than CMFs but much more than SBA-15 (Figure 13A). The increase concerning its source material (SBA-15) is logical due to the addition of the amino groups that interact with the CO₂ molecule. The lower amount adsorbed by CMFs may be due to a lower specific surface area. However, this material presents something remarkable with respect to CMFs and SBA-15. At low pressures, it adsorbs a more significant amount of CO₂ (Figure 13A), which directly causes different behavior in $\Delta_{ads}h$ (Figure 13B). CMFs and SBA-15 have very similar values for $\Delta_{ads}h$; the only difference is that CMFs presents values towards higher coverages because they adsorb a higher amount of CO₂, but both materials are in the interval of a physisorption process. In the case of the curve corresponding to SBA-15_APTES, the values begin at higher coverages because, at low pressures, it is adsorbing a greater amount of CO₂; in addition to that, the values are already at the limit between a physisorption and chemisorption process. Therefore, although CMFs adsorbs more CO₂ than SBA-15_APTES, it has lower interaction energy between adsorbate and adsorbent, making the material easier to regenerate. In SBA-15_APTES, where the interactions are stronger, perhaps some bonds will be more difficult to rupture. In conclusion, the values are at the limit between one and the other process. So, this does not rule out the use of SBA-15 amine-functionalized in industrial processes.

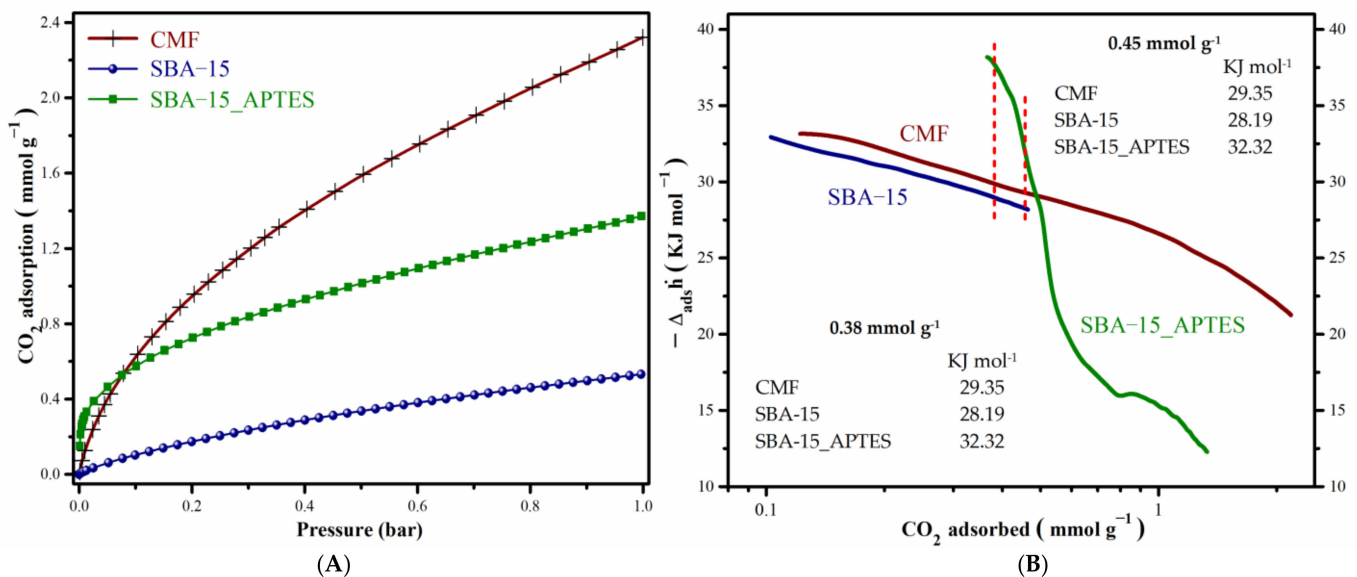


Figure 13. (A) CO₂ adsorption isotherms at 298 K. (B) Isothermic enthalpy of adsorption of CO₂ considering the nine CO₂ adsorption isotherms.

4. Conclusions

Calculating the isothermic enthalpy of adsorption of CO₂ using the CO₂ isotherms and the Clausius–Clapeyron equation allowed the identification of a physical or chemical process in the material studied, considering the effect of microporosity, mesoporosity, or surface chemistry. Some results worth emphasizing are:

- CMF is a microporous material with a specific surface area of 805 m² g⁻¹ and a chemical surface with nitrogen and oxygen functional groups, at 298 K and 1 bar; this material adsorbed 2.32 mmol CO₂ g⁻¹ with a $\Delta_{ads}h$ value of -30 KJ mol⁻¹ (a predominant process of physisorption).

- (b) SBA-15, a mesoporous material with a specific surface area of $735 \text{ m}^2 \text{ g}^{-1}$ and silanol groups in its surface, adsorbed $0.53 \text{ mmol CO}_2 \text{ g}^{-1}$ (at 298 K and 1 bar), about 25% of the total amount adsorbed by CMF, both materials have very similar specific surface areas, this difference could be due to the presence of micropores in CMFs. However, surface chemistry may play a more important role; different nitrogen and oxygen functional groups may have a higher affinity for the CO_2 molecule than the silanol groups. The $\Delta_{ads} \dot{h}$ was -29 KJ mol^{-1} , a value almost identical to that for CMFs, where a physisorption process is prevailing.
- (c) SBA-15_APTES, a mesoporous material, decreased the specific surface area from $735 \text{ m}^2 \text{ g}^{-1}$ to $389 \text{ m}^2 \text{ g}^{-1}$, which is due to the addition of amine groups by the (3-Aminopropyl)triethoxysilane (APTES) precursor improving CO_2 adsorption, rising from $0.53 \text{ mmol CO}_2 \text{ g}^{-1}$ to $1.37 \text{ mmol CO}_2 \text{ g}^{-1}$ (at 298 K and 1 bar); besides, this material has a $\Delta_{ads} \dot{h}$ of -38 KJ mol^{-1} , which means that the surface affinity of SBA-15_APTES with CO_2 molecule is stronger compared to CMF and SBA-15. This surface affinity makes it a preferential chemisorption process, resulting in the production of different behaviors.

Then, in the case of CMFs and SBA-15 materials, the dominant process is physisorption. In both cases, regardless of the arrangement selected to calculate the isosteric enthalpy of adsorption, the behavior is very similar when using various combinations of isotherms in the range analyzed in this work. However, in materials where chemisorption is present (SBA-15_APTES), the behavior of this state function is affected by the temperature range implemented to obtain it. Considering the interval studied here (263 K to 303 K), if the isotherms at low temperatures (263 K to 283 K) are used to obtain $\Delta_{ads} \dot{h}$, the values are shifted towards higher values based on the reference values; if the isotherms at high temperatures (283 K to 303 K) are used, the values are shifted towards smaller values.

Supplementary Materials: The following are available online at <https://www.mdpi.com/article/10.3390/jcs5040102/s1>, Figure S1. Thermogravimetric analysis of CMF, SBA-15, and SBA-15_APTES.

Author Contributions: Writing—original draft preparation, methodology, and investigation, R.O.-L.; resources, conceptualization, A.D.-O. and J.M.E.-S.; supervision, C.F.; writing—review and editing, I.J.P.-H. and A.C.-U. All authors have read and agreed to the published version of the manuscript.

Funding: This research was funded by the Consejo Nacional de Ciencia y Tecnología (CONACyT) and the project SIP-IPN 20211384 “Procesos Capilares en Materiales Nanoporosos: un Estudio Experimental y de Simulación”. ROL thanks CONACyT for the financial support, CVU: 442652.

Acknowledgments: To the network SEP-PROMEP “Diseno Nanoscópico y Textural de Materiales Avanzados”, with the Project “Síntesis y Físicoquímica de Materiales Mesoporosos” (UAM-I CA-31 Físicoquímica de Superficies). Our thanks to Laboratories of DRX (INFR-2011-1-163250), Resonancia Magnética Nuclear (M.C. Marco Antonio Vera Ramirez) and the Microscopia Electronica de Transmisión of the Universidad Autónoma Metropolitana-Iztapalapa.

Conflicts of Interest: The authors declare no conflict of interest.

References

1. Przepiórski, J.; Skrodzewicz, M.; Morawski, A. High temperature ammonia treatment of activated carbon for enhancement of CO_2 adsorption. *Appl. Surf. Sci.* **2004**, *225*, 235–242. [[CrossRef](#)]
2. Douglas, A.; Carter, R.E.; Li, M.; Pint, C.L. Toward Small-Diameter Carbon Nanotubes Synthesized from Captured Carbon Dioxide: Critical Role of Catalyst Coarsening. *ACS Appl. Mater. Interfaces* **2018**, *10*, 19010–19018. [[CrossRef](#)]
3. Zeleňák, V.; Badaničová, M.; Halamová, D.; Čejka, J.; Zukal, A.; Murafa, N.; Goerigk, G. Amine-modified ordered mesoporous silica: Effect of pore size on carbon dioxide capture. *Chem. Eng. J.* **2008**, *144*, 336–342. [[CrossRef](#)]
4. Boycheva, S.; Zgureva, D.; Lazarova, K.; Babeva, T.; Popov, C.; Lazarova, H.; Popova, M. Progress in the Utilization of Coal Fly Ash by Conversion to Zeolites with Green Energy Applications. *Materials* **2020**, *13*, 2014. [[CrossRef](#)] [[PubMed](#)]
5. Chaemchuen, S.; Alam Kabir, N.; Zhou, K.; Verpoort, F. Metal–organic frameworks for upgrading biogas via CO_2 adsorption to biogas green energy. *Chem. Soc. Rev.* **2013**, *42*, 9304–9332. [[CrossRef](#)] [[PubMed](#)]
6. Gan, Y.X.; Gan, J.B. Advances in Manufacturing Composite Carbon Nanofiber-Based Aerogels. *J. Compos. Sci.* **2020**, *4*, 73. [[CrossRef](#)]

7. Babu, D.J.; Lange, M.; Cherkashinin, G.; Issanin, A.; Staudt, R.; Schneider, J.J. Gas adsorption studies of CO₂ and N₂ in spatially aligned double-walled carbon nanotube arrays. *Carbon* **2013**, *61*, 616–623. [[CrossRef](#)]
8. Liou, T.-H.; Wang, P.-Y. Utilization of rice husk wastes in synthesis of graphene oxide-based carbonaceous nanocomposites. *Waste Manag.* **2020**, *108*, 51–61. [[CrossRef](#)]
9. Yan, X.; Komarneni, S.; Yan, Z. CO₂ adsorption on Santa Barbara Amorphous-15 (SBA-15) and amine-modified Santa Barbara Amorphous-15 (SBA-15) with and without controlled microporosity. *J. Colloid Interface Sci.* **2013**, *390*, 217–224. [[CrossRef](#)]
10. Rao, N.; Wang, M.; Shang, Z.; Hou, Y.; Fan, G.; Li, J. CO₂ Adsorption by Amine-Functionalized MCM-41: A Comparison between Impregnation and Grafting Modification Methods. *Energy Fuels* **2018**, *32*, 670–677. [[CrossRef](#)]
11. Thommes, M.; Kaneko, K.; Neimark, A.V.; Olivier, J.P.; Rodriguez-Reinoso, F.; Rouquerol, J.; Sing, K.S. Physisorption of gases, with special reference to the evaluation of surface area and pore size distribution (IUPAC Technical Report). *Pure Appl. Chem.* **2015**, *87*, 1051–1069. [[CrossRef](#)]
12. Lowell, S.; Shields, J.E.; Thomas, M.A.; Thommes, M. *Characterization of Porous Solids and Powders: Surface Area, Pore Size and Density*; Kluwer Academic Publishers: London, UK, 2004; ISBN 1-4020-2302-2.
13. Rouquerol, F.; Rouquerol, J.; Sing, K.S.W.; Llewellyn, P.; Maurin, G. *Adsorption by Powders and Porous Solids: Principles, Methodology and Applications*, 2nd ed.; Elsevier: New York, NY, USA, 2014; ISBN 9780080970356.
14. Builes, S.; Sandler, S.I.; Xiong, R. Isothermic Heats of Gas and Liquid Adsorption. *Langmuir* **2013**, *29*, 10416–10422. [[CrossRef](#)] [[PubMed](#)]
15. Nicholson, D.; Quirke, N. The role of isothermic enthalpy of adsorption in micropore characterisation: A simulation study. In *Studies in Surface Science and Catalysis*; Unger, K.K., Kreysa, G., Baselt, J.P., Eds.; Elsevier Science B.V.: Amsterdam, The Netherlands, 2000; Volume 128, pp. 11–20. ISBN 978-0-444-50259-9.
16. Sircar, S.; Mohr, R.; Ristic, C.; Rao, M.B. Isothermic Heat of Adsorption: Theory and Experiment. *J. Phys. Chem. B* **1999**, *103*, 6539–6546. [[CrossRef](#)] [[PubMed](#)]
17. Saha, D.; Grappe, H.A. Adsorption properties of activated carbon fibers. In *Activated Carbon Fiber and Textiles*; Chen, J.Y., Ed.; Elsevier Ltd.: Amsterdam, The Netherlands, 2017; pp. 143–165. ISBN 978-0-08-100660-3.
18. Zhao, D.; Feng, J.; Huo, Q.; Melosh, N.; Fredrickson, G.H.; Chmelka, B.F.; Stucky, G.D. Triblock copolymer syntheses of mesoporous silica with periodic 50 to 300 Å pores. *Science* **1998**, *279*, 548–552. [[CrossRef](#)]
19. Ojeda-López, R.; Pérez-Hermosillo, I.J.; Esparza-Schulz, J.M.; Cervantes-Uribe, A.; Domínguez-Ortiz, A. SBA-15 materials: Calcination temperature influence on textural properties and total silanol ratio. *Adsorption* **2015**, *21*, 659–669. [[CrossRef](#)]
20. Munguía-Cortés, L.; Pérez-Hermosillo, I.; Ojeda-López, R.; Esparza-Schulz, J.M.; Felipe-Mendoza, C.; Cervantes-Uribe, A.; Domínguez-Ortiz, A. APTES-functionalization of SBA-15 using ethanol or toluene: Textural characterization and sorption performance of carbon dioxide. *J. Mex. Chem. Soc.* **2017**, *61*, 273–281. [[CrossRef](#)]
21. Ojeda-López, R.; Esparza-Schulz, J.M.; Pérez-Hermosillo, I.J.; Hernández-Gordillo, A.; Domínguez-Ortiz, A. Improve in CO₂ and CH₄ Adsorption Capacity on Carbon Microfibers Synthesized by Electrospinning of PAN. *Fibers* **2019**, *7*, 81. [[CrossRef](#)]
22. Ladd, M.; Palmer, R. *Structure Determination by X-ray Crystallography: Analysis by X-rays and Neutrons*, 5th ed.; Springer US: New York, NY, USA, 2013; Volume 35, ISBN 978-1-4614-3954-7.
23. Brunauer, S.; Emmett, P.H.; Teller, E. Adsorption of Gases in Multimolecular Layers. *J. Am. Chem. Soc.* **1938**, *60*, 309–319. [[CrossRef](#)]
24. Rouquerol, J.; Llewellyn, P.; Rouquerol, F. Is the BET equation applicable to microporous adsorbents? *Stud. Surf. Sci. Catal.* **2007**, *160*, 49–56.
25. Kim, C.; Park, S.-H.; Cho, J.-I.; Lee, D.-Y.; Park, T.-J.; Lee, W.-J.; Yang, K.-S. Raman spectroscopic evaluation of polyacrylonitrile-based carbon nanofibers prepared by electrospinning. *J. Raman Spectrosc.* **2004**, *35*, 928–933. [[CrossRef](#)]
26. Zussman, E.; Chen, X.; Ding, W.; Calabri, L.; Dikin, D.; Quintana, J.; Ruoff, R. Mechanical and structural characterization of electrospun PAN-derived carbon nanofibers. *Carbon* **2005**, *43*, 2175–2185. [[CrossRef](#)]
27. Ojeda-López, R.; Ramos-Sánchez, G.; Esparza-Schulz, J.M.; Lartundo, L.; Domínguez-Ortiz, A. On site formation of N-doped carbon nanofibers, an efficient electrocatalyst for fuel cell applications. *Int. J. Hydrogen Energy* **2017**, *42*, 30339–30348. [[CrossRef](#)]
28. Kruk, M.; Jaroniec, M.; Sayari, A. Relations between Pore Structure Parameters and Their Implications for Characterization of MCM-41 Using Gas Adsorption and X-ray Diffraction. *Chem. Mater.* **1999**, *11*, 492–500. [[CrossRef](#)]
29. Kruk, M.; Jaroniec, M.; Joo, S.H.; Ryoo, R. Characterization of Regular and Plugged SBA-15 Silicas by Using Adsorption and Inverse Carbon Replication and Explanation of the Plug Formation Mechanism. *J. Phys. Chem. B* **2003**, *107*, 2205–2213. [[CrossRef](#)]
30. Ide, M.; El-Roz, M.; De Canck, E.; Vicente, A.; Planckaert, T.; Bogaerts, T.; Van Driessche, I.; Lynen, F.; Van Speybroeck, V.; Thybault-Starzyk, F.; et al. Quantification of silanol sites for the most common mesoporous ordered silicas and organosilicas: Total versus accessible silanols. *Phys. Chem. Chem. Phys.* **2013**, *15*, 642–650. [[CrossRef](#)] [[PubMed](#)]
31. Colilla, M.; Izquierdo-Barba, I.; Sánchez-Salcedo, S.; Fierro, J.L.G.; Hueso, J.L.; Vallet-Regí, M. Synthesis and Characterization of Zwitterionic SBA-15 Nanostructured Materials. *Chem. Mater.* **2010**, *22*, 6459–6466. [[CrossRef](#)]
32. Rahman, I.; Jafarzadeh, M.; Sipaut, C. Synthesis of organo-functionalized nanosilica via a co-condensation modification using γ -aminopropyltriethoxysilane (APTES). *Ceram. Int.* **2009**, *35*, 1883–1888. [[CrossRef](#)]
33. Chiang, Y.-C.; Lee, S.-T.; Leo, Y.-J.; Tseng, T.-L. Importance of Pore Structure and Surface Chemistry in Carbon Dioxide Adsorption on Electrospun Carbon Nanofibers. *Sensors Mater.* **2020**, *32*, 2277. [[CrossRef](#)]
34. Heo, Y.-J.; Zhang, Y.; Rhee, K.Y.; Park, S.-J. Synthesis of PAN/PVDF nanofiber composites-based carbon adsorbents for CO₂ capture. *Compos. Part B Eng.* **2019**, *156*, 95–99. [[CrossRef](#)]

35. Jeong, D.; Jie, W.; Adelodun, A.A.; Kim, S.; Jo, Y. Electrospun melamine-blended activated carbon nanofibers for enhanced control of indoor CO. *J. Appl. Polym. Sci.* **2019**, *136*, 3–10. [[CrossRef](#)]
36. Choma, J.; Stachurska, K.; Marszewski, M.; Jaroniec, M. Equilibrium isotherms and isosteric heat for CO₂ adsorption on nanoporous carbons from polymers. *Adsorption* **2016**, *22*, 581–588. [[CrossRef](#)]
37. Kamran, U.; Choi, J.R.; Park, S.-J. A Role of Activators for Efficient CO₂ Affinity on Polyacrylonitrile-Based Porous Carbon Materials. *Front. Chem.* **2020**, *8*, 710–727. [[CrossRef](#)]
38. Li, Y.; Zou, B.; Hu, C.; Cao, M. Nitrogen-doped porous carbon nanofiber webs for efficient CO₂ capture and conversion. *Carbon* **2016**, *99*, 79–89. [[CrossRef](#)]
39. Králik, M. Adsorption, chemisorption, and catalysis. *Chem. Pap.* **2014**, *68*, 1625–1638. [[CrossRef](#)]
40. de Ribeiro, J.; Nunes, E.H.M.; Vasconcelos, D.C.L.; Vasconcelos, W.L.; Nascimento, J.F.; Grava, W.M.; Derks, P.W.J. Role of the type of grafting solvent and its removal process on APTES functionalization onto SBA-15 silica for CO₂ adsorption. *J. Porous Mater.* **2019**, *26*, 1581–1591. [[CrossRef](#)]
41. Vilarrasa-García, E.; Moya, E.O.; Cecilia, J.; Cavalcante, C.; Jiménez-Jiménez, J.; Azevedo, D.; Rodríguez-Castellón, E. CO₂ adsorption on amine modified mesoporous silicas: Effect of the progressive disorder of the honeycomb arrangement. *Microporous Mesoporous Mater.* **2015**, *209*, 172–183. [[CrossRef](#)]
42. Cecilia, J.A.; Vilarrasa-García, E.; Morales-Ospino, R.; Bastos-Neto, M.; Azevedo, D.C.S.; Rodríguez-Castellón, E. Insights into CO₂ adsorption in amino-functionalized SBA-15 synthesized at different aging temperature. *Adsorption* **2020**, *26*, 225–240. [[CrossRef](#)]
43. Medina-Juárez, O.; García-Sánchez, M.Á.; Arellano-Sánchez, U.; Kornhauser-Straus, I.; Rojas-González, F. Optimal Surface Amino-Functionalization Following Thermo-Alkaline Treatment of Nanostructured Silica Adsorbents for Enhanced CO₂ Adsorption. *Materials* **2016**, *9*, 898. [[CrossRef](#)]
44. Ojeda-López, R.; Aguilar-Huerta, E.; Maia, D.A.S.; Azevedo, D.C.S.; Felipe, C.; Domínguez-Ortiz, A. Tailoring synthesis conditions of carbon microfibrils to enhance the microporosity, CO₂ and CH₄ adsorption by using the response surface methodology. *Microporous Mesoporous Mater.* **2020**, *305*, 110333–110341. [[CrossRef](#)]